

Swift heavy ion induced modifications in the structural, optical and methane sensing properties of indium oxide thin films - A comparative study using Ag^{9+} and O^{7+} ion irradiation

Riti Sethi¹, Anver Aziz¹, G.B.V.S. Lakshmi², D.K. Avasthi³ and Azher M. Siddiqui^{1*}

¹Department of Physics, Jamia Millia Islamia, New Delhi 110025

²Special Center for Nanosciences, Jawaharlal Nehru University, New Delhi 110067

³Amity Institute of Nanotechnology, Noida, Uttar Pradesh 201313

*Corresponding author

DOI: 10.5185/amlett.2018.2033

www.vbripress.com/aml

Abstract

Thin films of indium oxide grown on quartz substrates were subjected to 100 MeV Ag^{9+} and O^{7+} ions irradiation. The pristine and swift heavy ions irradiated films were characterized using X-ray Diffraction, Rutherford Backscattering Spectrometry, Scanning Electron Microscopy and UV-Vis Spectroscopy to examine the effect of irradiation with ions having large difference in the values of electronic energy loss (S_e) on the structural, microstructural and optical properties of indium oxide thin films. XRD and SEM studies revealed deterioration in crystallinity along with decrease in both crystallite size and grain size upon irradiation with both Ag^{9+} and O^{7+} ions. However, the decrease in the crystallite size and grain size in comparison to the pristine film was more radical for irradiation with Ag^{9+} ions. RBS spectra suggest that the electronic sputtering in the indium oxide films due to SHI irradiation is very less. AFM images illustrate the decrease in surface roughness from 29.8 nm for the pristine film to 27.4 nm and 26.7 nm on irradiation with 100 MeV O^{7+} and Ag^{9+} ions at a fluence of 3.3×10^{13} ions/cm². Also, UV-Vis study revealed an increment in the value of optical band gap from 3.41 eV for the pristine film to 3.53 and 3.67 eV for indium oxide films irradiated with of 3.3×10^{13} ions/cm² fluence of O^{7+} and Ag^{9+} ions respectively. The irradiation induced structural and optical modifications have been explained using the Thermal spike model. Along with the structural and optical properties, sensing properties of the pristine and irradiated films for 100 ppm methane gas at an operating temperature of 300°C have also been examined and the results have been correlated with the induced structural modifications. Copyright © 2018 VBRI Press.

Keywords: Indium oxide, swift heavy ions, electronic energy loss, thermal spike, gas sensing.

Introduction

The sensing properties of semiconducting metal oxides have been widely studied [1] because of the several advantageous features such as simplicity in device structure, low cost for fabrication, robustness in practical applications, and adaptability to a wide variety of reductive or oxidative gases [2]. The most extensively studied metal oxides for the application as gas sensors are ZnO [3-8] and SnO₂ [9-14]. Very little attention has been paid to the sensing properties of other metal oxides such as indium oxide.

This paper focuses on the methane sensing properties of indium oxide films deposited on quartz substrate. Also, swift heavy ion irradiation (SHI) has been employed as a tool to enhance the gas sensing properties of the as-deposited indium oxide films towards methane. SHI induced irradiation of materials has been established as one of the most effective techniques to induce modifications in the nanostructure

of materials [15-17] and therefore, is capable of altering the gas sensing properties of materials. On passage through the material, swift heavy ions lose their energy through inelastic collisions with the target electrons causing structural modifications such as amorphization, re-crystallization and phase changes [18]. The energy loss in this case is known as electronic energy loss (S_e). The two models that account for causing material modifications as a result of SHI irradiation are Coulomb explosion [18] and thermal spike model [19]. The Coulomb explosion model explains the formation of columnar defects in insulating materials occurring due to electrostatic repulsion of positive ions formed surrounding the ion path. On the other hand, the thermal spike model explains the formation of ion tracks and columnar defects within a narrow cylindrical zone in insulating as well as conducting materials for a duration of ~picoseconds as a result of passage of swift heavy ions through the material due to the temperature spike in that zone. The material modifications caused

due to swift heavy ion irradiation in turn affects the gas sensing characteristics of metal-oxides [20,21]. The electronic energy loss (S_e) values for Ag^{9+} and O^{7+} beam are 21.27 and 1.53 keV/nm respectively. This huge difference in the value of S_e accounts for the difference in the type and density of defects generated in the indium oxide film (with other factors such as beam energy and fluence being constant) which will in turn affect the modifications induced in the films upon irradiation. The present work aims at the study of modifications in indium oxide films under irradiation of two different ions (Ag^{9+} and O^{7+}) with large difference in the values of S_e . Subsequently, methane gas sensing is investigated in pristine and irradiated films.

Experimental

In_2O_3 films were prepared by thermal oxidation of In films deposited on quartz substrates by thermal evaporation at room temperature under a vacuum of 1.5×10^{-4} Pa. The deposition rate was fixed at 0.2 nm/sec and with the help of a quartz crystal thickness monitor, 100 nm thick In films were grown. After deposition, the In films were thermally oxidized at 500°C for 5 hrs under constant flow of oxygen. The thermally oxidized In films were then mounted on a ladder and placed in a high vacuum irradiation chamber [22,23]. To achieve homogenous irradiation, the ion beam of ~1mm diameter was scanned on an area of 1cm×1cm using an electromagnetic scanner. The samples were irradiated with 100 MeV Ag^{9+} and O^{7+} ions at different fluences of 3.3×10^{11} , 3.3×10^{12} and 3.3×10^{13} ions/cm² for both the ions using 15UD Pelletron tandem accelerator at Inter-University Accelerator Center, New Delhi. Ion irradiation causes huge electronic excitation and ionization. These effects modify different properties that have been discussed. The structural and phase analysis of the pristine and irradiated films were carried out using the X'Pert Pro Panalytical Diffractometer with CuK_{α} ($\lambda=1.5406\text{\AA}$) radiation in the 2θ range 25°- 60° at a step size of 2 secs and 1° glancing angle at AIRF, JNU, Delhi. Micro-structural characterization was performed using Zeiss Ultra 55 FE-SEM at an acceleration voltage of 5kV at IIT-Bombay under INUP Project. AFM measurements were performed using Pico Scan 210 Atomic Force Microscope at IIT Bombay under INUP project. Rutherford Backscattering measurements have been performed using the RBS-400 system with 1.7 Million Volt Pelletron Accelerator at IUAC, Delhi. The optical properties were studied using the double beam (Campsec 300) spectrometer in the wavelength range 200-800 nm at IUAC, Delhi. The response characteristics of the pristine and irradiated films towards methane gas were studied using the in-house setup at IISC, Bangalore named ALICAT-2 at an operating temperature of 300°C by measuring current as a function of time.

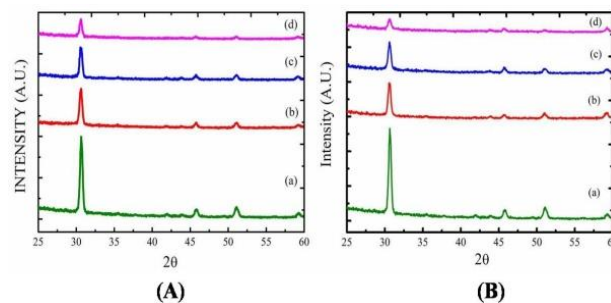


Fig. 1. XRD patterns of (A)(a) pristine In_2O_3 thin film and 100MeV O^{7+} SHI irradiated In_2O_3 films at fluence of (b) 3.3×10^{11} ions/cm², (c) 3.3×10^{12} ions/cm² and (d) 3.3×10^{13} ions/cm² and (B)(a) pristine In_2O_3 thin film and 100MeV Ag^{9+} SHI irradiated In_2O_3 films at fluence of (b) 3.3×10^{11} ions/cm², (c) 3.3×10^{12} ions/cm² and (d) 3.3×10^{13} ions/cm².

Results

Fig. 1(A) and **(B)** depict the XRD patterns of Ag^{9+} and O^{7+} ions irradiated indium oxide thin films respectively.

The XRD patterns presented in **Fig. 1** confirm the polycrystalline nature of In_2O_3 thin films. Also, the peaks with hkl values (222), (431), (440) and (541) match with the JCPDS file number 76-0152 belonging to cubic In_2O_3 .

It can be noticed that the diffraction patterns differ mainly on the peak intensities, full-width half maxima of the peaks and Bragg's peak position as we move from the pristine film to the one irradiated with highest fluence. The (222) peak is zoomed in and its variation with Ag^{9+} and O^{7+} ion fluence is shown in **Fig. 2(A)** and **(B)** respectively.

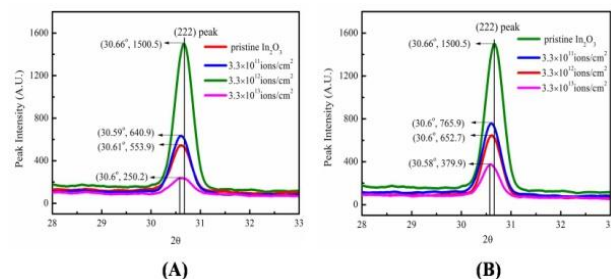


Fig. 2. Variation of (222) peak with (A) Ag^{9+} and (B) O^{7+} ion fluence.

With irradiation (both Ag^{9+} and O^{7+} ions), the indium oxide films retain their crystalline nature. However, the degree of crystallinity decreases with increase in the fluence of irradiation which is evident from the decrease in peak intensity and increase in the full-width half maxima for both Ag^{9+} and O^{7+} ions irradiation. The calculation of crystallite size [24] for the highest intensity peak (222) and the corresponding lattice strain [24] are performed using the formulae given in equations 1 and 2 respectively. The variation of crystallite size and lattice strain with Ag^{9+} and O^{7+} ion fluence is presented in **Figs. 3(A)** and **(B)** respectively.

$$D = \frac{\kappa\lambda}{\beta\cos\theta} \quad (1)$$

where, D is the crystallite size
 K is the shape factor with value close to unity
 λ is the wavelength of $CuK\alpha$ radiation, which is equal to 1.5406Å
 β is the full-width half maxima
 θ is the Bragg's angle

$$\text{Lattice strain} = \frac{K\lambda}{D} \quad (2)$$

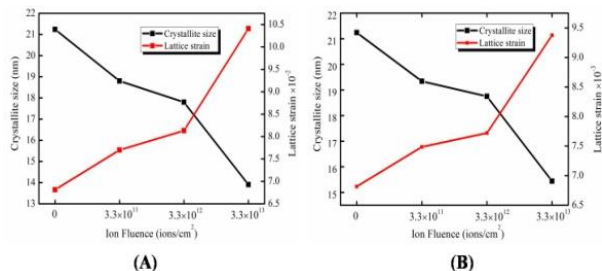


Fig. 3. Variation of crystallite size and lattice strain with 100 MeV (A) O⁷⁺ and (B) Ag⁹⁺ ion fluence for indium oxide thin films.

For irradiation with O⁷⁺ and Ag⁹⁺ ions, the crystallite size falls from 21.2 nm to 15.4 nm and 13.9 nm respectively. Also, the strain in the films increases with increase in the fluence of irradiation for both Ag⁹⁺ and O⁷⁺ ions.

The microstructural changes in the indium oxide films due to irradiation have been presented in **Fig. 4(A)** and **(B)** respectively with respect to the pristine film.

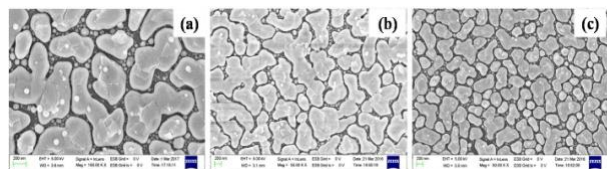


Fig. 4(A). SEM micrographs of (a) pristine In₂O₃ film and 100MeV O⁷⁺ ions irradiated In₂O₃ thin films at a fluence of (b) 3.3x10¹¹ ions/cm² and (c) 3.3x10¹³ ions/cm².

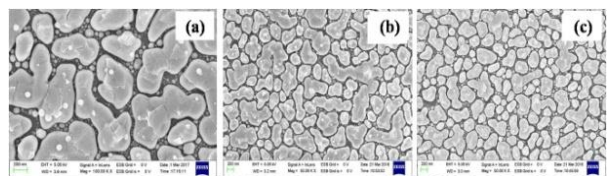


Fig. 4(B). SEM micrographs of (a) pristine In₂O₃ film and 100MeV Ag⁹⁺ ions irradiated In₂O₃ thin films at a fluence of (a) 3.3x10¹¹ ions/cm² and (c) 3.3x10¹³ ions/cm².

The micrographs depict grain fragmentation as a result of swift heavy ion irradiation that causes a decrease in the grain size. The variation of grain size with fluence is presented in Table 1.

Fig. 5 portrays the fluence dependent RBS spectra of indium oxide thin films irradiated with 100 MeV Ag⁹⁺ and O⁷⁺ ions with respect to the pristine film.

The RBS measurements were performed using He⁺⁺ ions at an energy of 2 MeV. The value of charge was fixed at 12 μC for the measurement. The RBS spectra show distinct peaks of O, Si and In for pristine

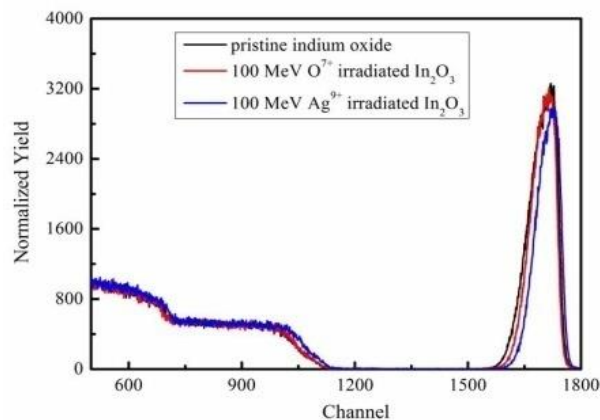


Fig. 5. RBS spectra of pristine In₂O₃ and 100MeV O⁷⁺ and Ag⁹⁺ SHI irradiated In₂O₃ film at fluence of 3.3x10¹³ ions/cm².

and irradiated samples. The decrease in the width of the indium peak upon irradiation is very less which implies that the electronic sputtering yield is very low. This is because the films are stoichiometric in nature and therefore, rate of electronic sputtering is very low. This implies that the morphological changes are due to surface diffusion induced by surface smoothening [25].

To attribute the morphological changes to surface diffusion, AFM study was carried out on the pristine and irradiated indium oxide films. The AFM images of the pristine and irradiated films presented in **Fig. 6(A, B and C)** show a decrease in the RMS roughness of the indium oxide films as we go from the pristine to the irradiated films.

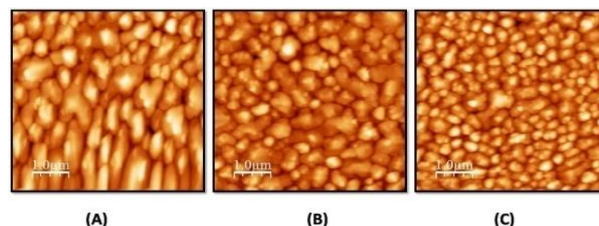


Fig. 6. AFM images of (A) pristine and 100 MeV (B) O⁷⁺ and (C) Ag⁹⁺ ions irradiated indium oxide film at a fluence of 3.3x10¹³ ions/cm².

The RMS roughness as calculated using WSXM software [26] for the pristine film was 29.8 nm. The value of roughness decreased to 27.4 nm and 26.7 nm on irradiation with 100 MeV O⁷⁺ and Ag⁹⁺ ions at a fluence of 3.3x10¹³ ions/cm².

The optical studies on pristine and 100MeV O⁷⁺ ions irradiated In₂O₃ films were carried out using UV-Vis Spectrometry. The optical band gap values were obtained from plots between (αhv)² and energy (hv) known as Tauc's plots. The relationship [27] used to obtain Tauc's plot is given as:

$$\alpha hv = B(hv - E_g)^n \quad (3)$$

where, α is the optical absorption coefficient

E_g is the optical band gap of the material

B is the transition probability that is dependent on the material and hv is the photon energy in eV.

The transition processes are governed by the value 'n' in the Tauc's relation. Depending upon the nature of transition, it can take values 1/2, 3/2, 2 and 3 for direct allowed, direct forbidden, indirect allowed and indirect forbidden transitions respectively [28]. For our band gap calculations, we select $n=1/2$ since the absorption coefficient is of the order of 10^4cm^{-1} (not shown) for both pristine and irradiated In_2O_3 . This supports the direct band gap nature of In_2O_3 [29]. The variation of optical band gap with Ag^{9+} and O^{7+} ion fluence is illustrated in Fig. 7(A) and (B) respectively.

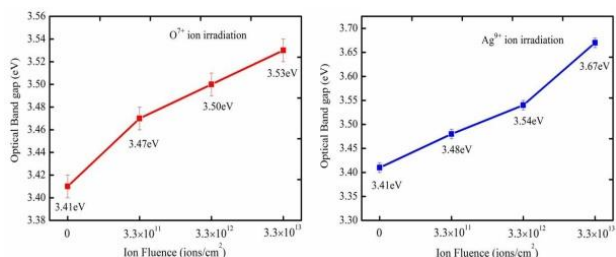


Fig. 7. Variation of optical band gap with 100 MeV (A) O^{7+} ion fluence and (B) Ag^{9+} ion fluence.

It is worth noticing that indium oxide films experience blue shift of the optical band gap due to irradiation with 100 MeV Ag^{9+} and O^{7+} ions. The optical band gap increases from 3.41 eV to 3.53 eV on irradiation with Ag^{9+} ions and on the other hand the optical band gap widening is much more in case of irradiation with 100 MeV O^{7+} ions where the value increases from 3.41 eV to 3.67 eV.

The current versus time curves for pristine and 100 MeV O^{7+} ions irradiated In_2O_3 films (fluence = 3.3×10^{13} ions/cm²) is shown in figure 8(A - C). These curves were utilized to calculate the values of sensitivity, response and recovery times. Fig. 8 (A), (B) and (C) show the variation of sensitivity, response time and recovery time of 100 MeV Ag^{9+} and O^{7+} ions irradiated films as a function of ion fluence respectively. The measurements were performed at an operating temperature of 300°C.

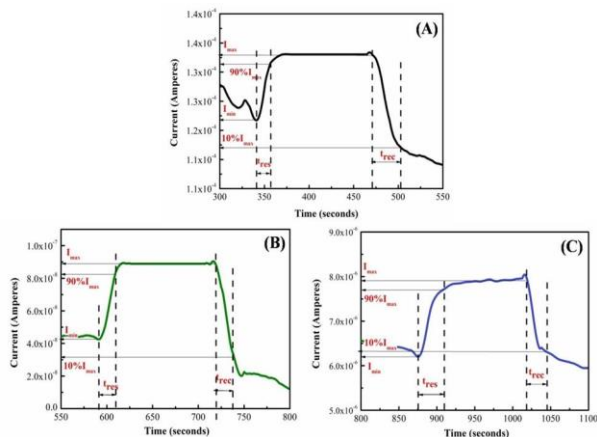


Fig. 8. Variation of current with time on exposure to 100 ppm methane gas for (A) pristine In_2O_3 film and 100 MeV (B) Ag^{9+} and (C) O^{7+} ions irradiated In_2O_3 films at a fluence of 3.3×10^{13} ions/cm².

The typical structure of the sensor used for the experiments consists of the In_2O_3 sensing layer upon the insulating substrate (quartz). Ag^{9+} dots were applied on the sensing layer that act as the electrodes for two probe conductance measurements. A heater was also placed under the substrate holder to attain an operating temperature of 300°C for the activation of sensor and its enhanced performance [20]. The sensing mechanism of polycrystalline In_2O_3 has been investigated by many researchers and the most commonly stated mechanism is based on the variation of surface electron depletion layer due to the reaction between the target gas and chemisorbed oxygen on the surface [21]. The sensitivity [17] has been calculated using the equation:

$$S = \frac{G_g - G_a}{G_a} \% \quad (4)$$

where, G_g and G_a represent conductance in gas and conductance in air respectively.

As seen from Fig. 9(A), the sensitivity towards methane increases with increase in the fluence for both Ag^{9+} and O^{7+} ions. However, the response towards methane gas is significantly higher on irradiation with Ag^{9+} ions as compared to O^{7+} ions. The sensor response hikes up to ~108.5% at the highest fluence of Ag^{9+} ions while it reaches only up to ~27.2% at the highest fluence of O^{7+} ions from ~9% for the pristine film. The response time (Fig. 9(B)) and the recovery time (Fig. 9(C)) of the indium oxide based sensor film towards methane gas is much lower in films irradiated with Ag^{9+} ions in comparison to the ones irradiated with O^{7+} ions. Therefore, if we compare the response characteristics of the indium oxide films irradiated with 100 MeV O^{7+} ions to the ones irradiated with 100 MeV Ag^{9+} ions, we observe that the indium oxide films irradiated with Ag^{9+} ions prove to show better response characteristics.

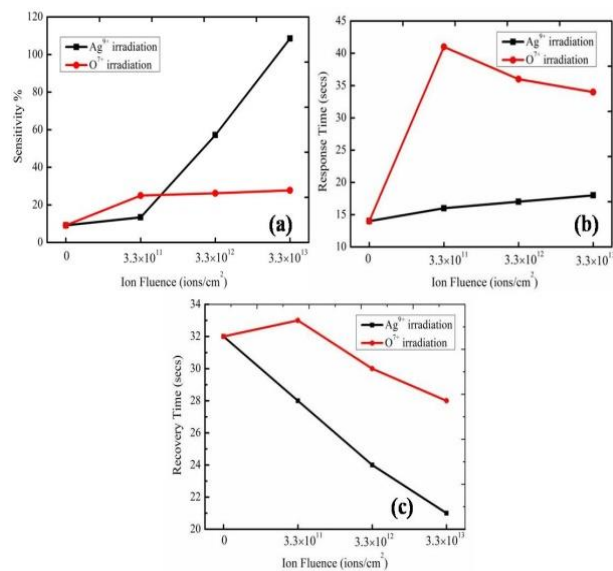


Fig. 9. Variation of (a) sensitivity, (b) response time and (c) recovery time with ion fluence for 100 MeV Ag^{9+} and O^{7+} ions irradiated indium oxide thin films.

Discussion

The electronic energy loss (S_e) obtained using SRIM [30] for 100 MeV Ag^{9+} and O^{7+} incident on indium oxide films were found to be 21.27 and 1.53 keV/nm respectively. These values are much larger than the corresponding nuclear energy loss values (S_n): 0.13 keV/nm for Ag^{9+} ions and 8.8×10^{-4} keV/nm for O^{7+} ions. This implies that the modifications induced in the properties of indium oxide thin films as a result of swift heavy ion irradiation are due to electronic excitations.

In the present study, we have employed the Thermal Spike model to explain the swift heavy ion induced modifications. According to the thermal spike model, the target material comprises of two subsystems: the electronic and atomic (lattice). The incident swift heavy ions interact with the electronic subsystem and the energy is transferred to the electrons of the target in a time which is less than 10^{-16} s [31]. Since, the time interval of the electron-ion interaction is very small, the lattice does not respond in this time scale. Between the time scales of 10^{-14} to 10^{-12} s, the energy is transferred from the electronic subsystem to the lattice. The coupling process is described by two differential equations. This process of transfer of energy results in a temperature rise in a narrow cylindrical zone along the ion path that quenches rapidly resulting in the formation of cylindrical regions known as latent tracks. The latent track zone may or may not be completely amorphous but is definitely different from its surroundings. Also, as per the velocity effect slower ions ($E/A < 2$ MeV amu^{-1}) are much more efficient at ion track formation than faster ions ($E/A > 8$ MeV amu^{-1}) [32,33]. For Ag^{9+} ions, $E/A = 0.92$ MeV amu^{-1} and for O^{7+} ions, $E/A = 6.25$ MeV amu^{-1} . On comparing the values of E/A for both Ag^{9+} and O^{7+} ions, we can conclude that Ag^{9+} ions have a very high probability of forming ion tracks in indium oxide films in comparison to O^{7+} ions. In another approach of thermal spike, given by Szenes et al [34], for the formation of latent tracks in the target material, it is necessary that the electronic energy loss is greater than the threshold electronic energy loss, that is, $S_e > S_{eth}$ with an efficient electron-phonon coupling, 'g' basically determines the ability of electrons to transfer their energy to the lattice and depends upon the velocity of the impinging ion. The value of 'g' taken in the present study is 0.4 [33]. To calculate the value of S_{eth} for indium oxide films, the following equation [34] can be used:

$$S_{eth} = \pi \rho c a^2(0) T_0 / g$$

From the above equation it can be seen that the value of S_{eth} depends upon the material parameters such as:

density of the material, ρ ($=7.17$ gcm^{-3})

average specific heat, c ($=0.0889$ $Jg^{-1}K^{-1}$)

the temperature rise in the thermal spike, T_0 ,

$$T_0 = T_m - T_{irr}$$

where, T_m is the melting point of indium oxide film ($=2190$ K [35]) and

T_{irr} is the irradiation temperature ($=293$ K) initial width of the thermal spike, $a(0)$ and electron-phonon coupling, g

It has been observed that the value of $a(0)$ depends upon the optical band gap (E_g) for semiconductors. The value of $a(0)$ used for the present study has been calculated elsewhere [36] and is equal to 4.5 nm for wide band gap semiconductors. Substituting the values of the mentioned parameters in equation (8), the value of S_{eth} comes out to be 1.192 keV/nm. Comparing the values of S_e for both Ag^{9+} and O^{7+} ions with the value of S_{eth} , we observe that track formation is possible in indium oxide films upon irradiation with Ag^{9+} as well as O^{7+} ions.

The track radius, R_e can be calculated using the following equation [34]:

$$R_e^2 = a^2(0) \ln \left(\frac{S_e}{S_{eth}} \right); \quad 1 \leq \frac{S_e}{S_{eth}} \leq 2.7$$

$$= [a^2(0)/2.7] \frac{S_e}{S_{eth}}; \quad \frac{S_e}{S_{eth}} > 2.7$$

The value of $\frac{S_e}{S_{eth}} \sim 17.87$ for Ag^{9+} ions irradiation and is equal to 1.28 for O^{7+} ions irradiation. The track radii were calculated using equations 7 (a) and (b) for irradiation with 100 MeV O^{7+} and Ag^{9+} ions respectively and the values obtained were 2.25 and 11.6 nm. The huge difference in the values of track radius can be attributed to the large difference in the values of S_e of Ag^{9+} and O^{7+} ions and also to the velocity effect. The reduction in track sizes at high SHI velocities can be related to the low density of the deposited energy due to the high energy of scattered electrons which results in a monotonically increasing threshold for track formation with ion velocity [37,38]. On the other hand, for low swift heavy ion velocities (below 2MeV amu^{-1}), the track sizes obtained are large which are attributed to a contribution from Coulomb explosion [39,40]. Also, the 1 cm^2 sample will be fully covered with melted zones/latent tracks at a Ag^{9+} ion fluence of $\sim 2 \times 10^{11}$ ions/ cm^2 and O^{7+} ion fluence of $\sim 6 \times 10^{12}$ ions/ cm^2 , corresponding to $1/\pi R_e^2$ [41].

Beyond this critical fluence, there will be considerable overlapping of melted zones. The values of critical fluence suggest that the indium oxide films irradiated with O^{7+} ions will be covered completely with melted zones at the highest fluence of 3.3×10^{13} ions/ cm^2 whereas, complete coverage of indium oxide films with melted zones on irradiation with Ag^{9+} ions will be observed even at the lowest fluence of 3.3×10^{11} ions/ cm^2 . Therefore, the extent of amorphization is more pronounced in the case of irradiation with Ag^{9+} ions as also suggested from the XRD patterns presented in figure 1(A). Also, the magnitude of reduction in the crystallite size is higher in the films irradiated with Ag^{9+} ions (21.2 - 13.9 nm) than the films irradiated with O^{7+} ions (21.2 - 15.4 nm) as seen from Figs. 2 and 3. The microstructural changes in the indium oxide films due to O^{7+} and Ag^{9+} ions irradiation with respect to the pristine film are presented in the SEM micrographs

illustrated in figures 4(A) and (B). The micrographs clearly depict a reduction in the grain size due to irradiation. The SHI induced grain fragmentation is due to the strain produced in the films as a result of the temperature spike along and in the vicinity of the ion path. This temperature spike results in the development of pressure waves that causes strain in the grains resulting in a decrease of the grain size. The grain fragmentation due to SHI irradiation has also been reported by Kumar et al [42]. Since, the magnitude of lattice strain is one order higher in the indium oxide films irradiated with 100 MeV Ag^{9+} ions than their O^{7+} ions counterpart (Figs. 3(A) and (B)), therefore, the grain fragmentation is much more radical in the films irradiated with Ag^{9+} ions (281.9 nm - 144.1nm) than in the films irradiated with O^{7+} ions (281.9 nm - 204.5nm). Furthermore, the optical band gap widening as a result of SHI (Ag^{9+} and O^{7+}) irradiation illustrated in figure 7 can be attributed to quantum confinement effect [43] according to which the absorption edge shifts to higher energy with decrease in crystallite size which leads to an increase in the value of optical band gap. The enhancement in the sensing response on irradiation with both O^{7+} and Ag^{9+} ions (figure 9(A)) can be attributed to the reduction in the crystallite size due to which the number of active sites available for adsorption of gas molecules increases because of the increase in surface area [17]. However, the magnitude of enhancement of sensing response is much larger in the case of irradiation with Ag^{9+} ions than with O^{7+} ions (more than 3 times larger at the highest fluence) which is possibly due to significantly greater surface modifications induced due to Ag^{9+} ions irradiation in contrast to the modifications induced by O^{7+} ions like crystallite size and grain size reduction as seen from the XRD and SEM images.

Conclusions

The effect of the value of electronic energy loss on the structural and optical properties of indium oxide thin films irradiated with 100 MeV Ag^{9+} ($S_e = 21.27$ keV/nm) and O^{7+} ($S_e = 1.53$ keV/nm) ions has been examined. It has been observed that both Ag^{9+} and O^{7+} ions result in the formation of ion tracks in indium oxide films. However, the radius of tracks formed by Ag^{9+} ions is much higher than those formed by O^{7+} ions due to a large difference in the values of their electronic energy losses. This results in more radical modifications in the structural and optical properties of indium oxide thin films in comparison to the films irradiated with O^{7+} ions. The morphological evolution of the indium oxide films upon irradiation with Ag^{9+} and O^{7+} ions has been attributed to surface diffusion caused due to surface smoothening as seen from the AFM images. The study of sensing properties towards 100 ppm methane gas revealed an increase in the sensing response from a mere 9% for pristine film to ~27.2% and 108.5% upon irradiation with 100 MeV O^{7+} and Ag^{9+} ions respectively at a fluence of 3.3×10^{13}

ions/cm². We therefore conclude that irradiation with Ag^{9+} ions has a more drastic effect on the properties of indium oxide thin films.

Acknowledgements

One of the authors (Ms Riti Sethi) is thankful to the University Grants Commission (UGC), New Delhi for providing with the UGC-BSR Fellowship for carrying out this research work. The authors are also thankful to Pelletron Accelerator group, Mr Sunil Ojha and Mr G.R. Umapathy at IUAC, Delhi for support during ion beam and RBS experiments. The authors would also like to acknowledge the support of INUP for carrying out research work at CEN and CENSE at IIT-Bombay and IISC, Bangalore respectively.

References

- Gnanasekar, K.I; Prabhu, E; Jayaraman, V; Gnanasekaran, T; *Advanced Materials Letters*, **2013**, 4(6), 464
- Chung, W.Y; Sakai, G; K. Shimano, K; Miura, N; Lee, D. D; Yamazoe, N; *Sensors and Actuators B*, **1998**, 46, 139
- Hosseinejad, M.T; Shirazi, M; Ghoranneveiss, M; Hantehzadeh, M. R; Darabi, E; *Journal of Inorganic and Organometallic Polymers and Materials*, **2016**, 26, 405
- Lim, H.J; Lee, D.Y; Oh, Y.J; *Sensors and Actuators A*, **2006**, 125, 405
- Suchea, M; Christoulakis, S; Moschovis, K; Katsarakis, N; Kiriakidis, G; *Thin Solid Films*, **2006**, 515, 551
- Shishiyanu, S.T; Shishiyanu, T.S; Lupan, O.I; *Sensors and Actuators B*, **2005**, 107, 379
- Gong, H; Hu, J.Q; Wang, J.H; Ong, C.H; Zhu, F.R; *Sensors and Actuators B*, **2006**, 115, 247
- Dimitrov, I.G; Dikovska, A.O; Atanasov, P.A; Stoyancho, T.R; Vasilev, T; *Journal of Physics: Conference Series*, **2008**, 113, 012044
- Huo, H.B; Wang, C; Yan, F.D; Ren, H.D; Shen, M.Y; *Journal of Nanoscience and Nanotechnology*, **2009**, 9(8), 4817
- Nath, R.K; Nath, S.S; *Sensors and Materials*, **2009**, 21(2), 95
- Kadhim, I.H; Hassan, M.A; Abdullah, Q.N; *Nano-Micro Letters*, **2016**, 8(1), 20
- Khanna, A; Kumar, R; Bhatti, S.S; *Applied Physics Letters*, **2003**, 82(24), 4388
- Ray, S; Gupta, P.S; Singh, G; *Journal of Ovonic Research*, **2010**, 6(1), 63
- Sinha, S.K; *Advanced Materials Letters*, **2015**, 6(2), 133
- Jaiswal, M.K; Kumar, A; Kanjilal, D; Mohanty, T; *Applied Surface Science*, **2012**, 263, 586
- Negi, S; Rana, M.P.S; Singh, F; Ramola, R.C; *Journal of Sol-Gel Science and Technology*, **2015**, 76(3), 608
- Singh, R.C; Singh, M.P; Singh, O; Chandi, P.S; Kumar, R; *Applied Physics A*, **2010**, 98, 161
- Fleischer, R.L; Price, P.B; Walker, R.M; *Journal of Applied Physics*, **1965**, 36, 3645
- Seitz, F; Koehler, J.S; *Solid State Physics*, **1956**, 2, 305
- Rani, S; Roy, S.C; Puri, N.K; Bhatnagar, M.C; Kanjilal, D; *Journal of Nanomaterials*, **2008**, Article ID 395490, 4 pages
- Baly, A.K; Singh, R; Bedi, R.K; *Journal of Material Science and Technology*, **2012**, 28(8), 700
- Sethi, R; Kumar, P; Khan, S.A; Aziz, A; Siddiqui, A.M; *AIP Conference Proceedings*, **2016**, 1742, 030016
- Sethi, R; Kaushik, P; Aziz, A; Siddiqui, A.M; Kumar, P; *Surface and Interface Analysis*, **2017**, 49, 910
- Klug, H.P; Alexander, L.E; *X-ray Diffraction Procedures for Polycrystalline and Amorphous Materials*, Wiley, New York, **1974**
- Tripathi, N; Tripathi, A; Rath, S; *Radiation Effects and Defects*, **2011**, 166(8-9), 578
- Horcas, I; Fernández, R; Gómez-Rodríguez, J.M; Colchero, J; Gómez-Herrero, J; Baro, A.M; *Review of Scientific Instruments*, **2007**, 78, 013705
- Tumuluri, A; Naidu, K.L; Raju, K.C.J; *International Journal of ChemTech Research*, **2014**, 6(6), 3353
- Jaiswal, M.K; Kanjilal, D; Kumar, R; *Nuclear Instruments and Methods in Physics Research B*, **2013**, 314, 170

29. Palanichamy, S; Amalraj, L; Mohamed, J.R; Kumar, P.S.S; *South Asian Journal of Engineering and Technology*, **2016**, 2(14), 26
30. Ziegler, J.F; Biersak, J.P; Littmark, U; Stopping and Range of Ions in Solids, Pergamon, New York, **1985**
31. Toulemonde, M; Dufour, C; Paumier, E; *Physical Review B*, **1992**, 46(22), 14362
32. Toulemonde, M; Trautmann, C; Balanzat, E; Hjort, K; Weidinger, A; *Nuclear Instruments and Methods in Physics Research B*, **2004**, 216, 1
33. Meftah, A; Brisard, F; Costantini, J.M; Hage-Ali, M; Stoquert, J.P; Studer, F; Toulemonde, M; *Physical Review B*, **1993**, 48(2), 920
34. Szenes, G; *Physical Review B*, **1995**, 51, 8026
35. Batzill, M; Diebold, U; *Progress in Surface Science*, **2005**, 79, 47
36. Szenes, G; Horvath, Z.E; Pécze, B; Pászti, F; Tóth, L; *Physical Review B*, **2002**, 65, 045206-(1)
37. Toulemonde, M; Assmann, W; Dufour, C; Meftah, A; Trautmann, C; *Nuclear Instruments and Methods in Physics Research B*, **2012**, 277, 28
38. Toulemonde, M; Assmann, W; Dufour, C; Meftah, A; Trautmann, C; *Mat.-Fys. Medd. Dan. Vidensk. Selsk.*, **2006**, 52, 263
39. Szenes, G; *Nuclear Instruments and Methods in Physics Research B*, **2011**, 269, 174
40. Szenes, G; *Nuclear Instruments and Methods in Physics Research B*, **2013**, 298, 76
41. Gupta, S; Singh, F; Sulania, I; Das, B; *Surface Science*, **2017**, 664, 137
42. Kumar, M; Singh, F; Khan, S.A; Baranwal, V; Kumar, S; Agarwal, D.C; Siddiqui, A.M; Tripathi, A; Gupta, A; Avasthi, D.K; Pandey, A.C; *Journal of Physics D: Applied Physics*, **2005**, 38, 637
43. Kim, H; Gilmore, C.M; Piqué, A; Horwitz, J.S; Mattoussi, H; Murata, H; Kafafi, Z.H; and Chrisey, D.B; *Journal of Applied Physics*, **1999**, 86(11), 6451.